

# UC Davis

## UC Davis Previously Published Works

### Title

Triangular cross-section beam splitters in silicon carbide for quantum information processing

### Permalink

<https://escholarship.org/uc/item/100833jr>

### Journal

MRS Communications, 14(6)

### ISSN

2159-6859

### Authors

Majety, Sridhar

Saha, Pranta

Kekula, Zbynka

et al.

### Publication Date

2024-12-01

### DOI

10.1557/s43579-024-00557-0

### Copyright Information

This work is made available under the terms of a Creative Commons Attribution License, available at <https://creativecommons.org/licenses/by/4.0/>

Peer reviewed

# Triangular Cross-Section Beam Splitters in Silicon Carbide for Quantum Information Processing

Sridhar Majety <sup>\*†1</sup>, Pranta Saha <sup>†1</sup>, Zbynka Kekula<sup>1</sup>, Scott Dhuey<sup>2</sup>, and Marina Radulaski<sup>1</sup>

<sup>1</sup>*Department of Electrical and Computer Engineering, University of California, Davis, CA 95616, USA*

<sup>2</sup>*The Molecular Foundry, Lawrence Berkeley National Laboratory, Berkeley, CA 94720, USA*

## Abstract

Triangular cross-section color center photonics in silicon carbide is a leading candidate for scalable implementation of quantum hardware. Within this geometry, we model low-loss beam splitters for applications in key quantum optical operations such as entanglement and single-photon interferometry. We consider triangular cross-section single-mode waveguides for the design of a directional coupler. We optimize parameters for a 50:50 beam splitter. Finally, we test the experimental feasibility of the designs by fabricating triangular waveguides in an ion beam etching process and identify suitable designs for short-term implementation.

## 1 Introduction

Photonic quantum information processing (QIP) using solid-state single photon emitters has been extensively explored for applications in quantum communications and integrated quantum information circuits. Among the quantum emitters, color centers have been desired solid state qubit candidates due to their spectral homogeneity, long spin coherence times, and availability of spin-spin and spin-photon entangling processes, necessary for QIP applications [1–6]. Particularly, color centers in silicon carbide (SiC) attracted attention because of emissions in the telecommunication bands which are suitable for sending over

---

\*Corresponding author: smajety@ucdavis.edu

† These authors contributed equally to this work

long distances in fiber optic cable. SiC offers other advantages like large bandgap, strong second-order non-linearity, decades-long industry presence, and is CMOS compatible.

The existing QIP algorithms require error correction and heralded measurements to process information reliably and efficiently. Hence, one of the near-term goals is to build the on-chip programmable photonic mesh networks to perform fault-tolerant QIP [7–9]. Successful implementation of such quantum mesh photonic hardware requires efficient single photon generation, manipulation, entanglement, and detection [10–12]. Beamsplitters (BS) play a crucial role in on-chip photonic QIP circuits for generating multiphoton correlation [8, 13] and can be used to realize several important operations like entanglement generation and single-photon interferometry (Hong-Ou-Mandel and Hanbury Brown-Twiss). Moreover, a universal quantum computer with linear optical quantum computing protocols has been proposed using BS, phase shifters, single photon sources, and photo-detectors [14]. Among the most studied forms of BS such as Y-branch, directional coupler (DC), and multi mode interferometer (MMI), DC is the most suited for on-chip QIP as it can function with single-mode waveguides [15].

Color centers properties are preserved in the bulk of the host material and for successful nanophotonic integration of these color centers, it is necessary to be able to grow or attach a high quality thin film on a substrate with high refractive index contrast in a scalable way. Triangular photonics has been the top choice in diamond, silicon carbide and rare earth photonics [16–18] that provides pristine color centers and high light and matter interaction. Compared to the other non-traditional processing techniques [19–21] used for fabricating undercut devices, angle etching method [16, 18, 22] which produces triangular cross-section and undercut photonic devices, is promising for wafer-scale production [23]. Performance of a variety of such triangular cross-section photonic structures in 4H-SiC were recently examined [12, 18, 24, 25], and have proven favorable for QIP applications.

In this paper, we explore triangular cross-section 50:50 BS in 4H-SiC necessary for performing on-chip quantum interferometry. We construct such a device that splits an input beam into two output beams of equal intensity using two concurrent waveguides. In the front and back regions, the waveguides are far apart (no electromagnetic interaction) on either ends (input, output) of the device, while in the middle overlap region waveguides propagate in close proximity to create an electromagnetic interaction between their fields. When two

indistinguishable photons each entangled to a spin of a quantum emitter arrive at the inputs of a 50:50 BS at the same time, they undergo bunching to exit together through the same output, creating remote entanglement between the two spins. Here we specifically study 50:50 BS designs for nitrogen vacancy (NV) color centers in 4H-SiC, with single photon emissions in the telecommunication wavelength range (1176 - 1243 nm) [26,27].

Using Finite-Difference Time-Domain (FDTD) method, we first optimize the width of triangular cross-section waveguides to achieve single mode propagation (fundamental TE mode), and high coupling efficiency of the color center (NV in 4H-SiC) emission into that single mode, for different etch angles. Next, we investigate the formation of supermodes when two identical single mode waveguides are placed adjacent to each other. We then study the waveguide mode conversion in bent waveguides and find suitable waveguide bend geometries to maintain the same waveguide mode in the straight and bent regions of the waveguide. We use this understanding to design triangular cross-section 50:50 BS in 4H-SiC. Finally, we explore the fabrication of the simulated triangular cross-section waveguide configurations required for a 50:50 BS.

## 2 Single mode triangular cross-section waveguide

Color center emission is dipole-like and such emission can couple to fundamental TE (f-TE), fundamental TM (f-TM) and other higher order modes that are supported in triangular cross-section waveguides [24]. It has been shown that for each etch angle there exists an optimal width for single mode (f-TE) propagation in triangular cross-section waveguides [18], which is a necessity for QIP applications [28]. So, to achieve high coupling efficiencies for color center emission, the color center should be positioned in a single mode waveguide at the maximum electric field (E-field) intensity point of the f-TE mode [12, 18], which is at the centroid of the triangle.

We use FDTD package in Lumerical software to estimate the coupling efficiency of color center emission into the f-TE mode ( $C_{fTE}$ ) for different widths ( $w$ ) and etch angles ( $\alpha$ ) of a triangular cross-section waveguide (the angle at the apex of the triangle is  $2\alpha$ ). We position the dipole emitter at the centroid of the triangle with an emission wavelength of 1230 nm.



We find that for each  $\alpha$  there exists a width with highest coupling ( $> 80\%$ ) to the f-TE mode as shown in Figure 1. For our 50:50 BS simulations, we choose the optimal width values ( $w = 550$  nm,  $650$  nm,  $800$  nm for  $\alpha = 30^\circ, 45^\circ, 60^\circ$  respectively) slightly lower than the widths with the highest  $C_{\text{fTE}}$ . The reason being that the waveguides with lower width have slightly higher evanescent fields (top panels of inset in Figure 1), necessary to create meaningful coupling between the adjacent waveguides in the BS, while only slightly reducing  $C_{\text{fTE}}$  ( $< 1\%$ ).

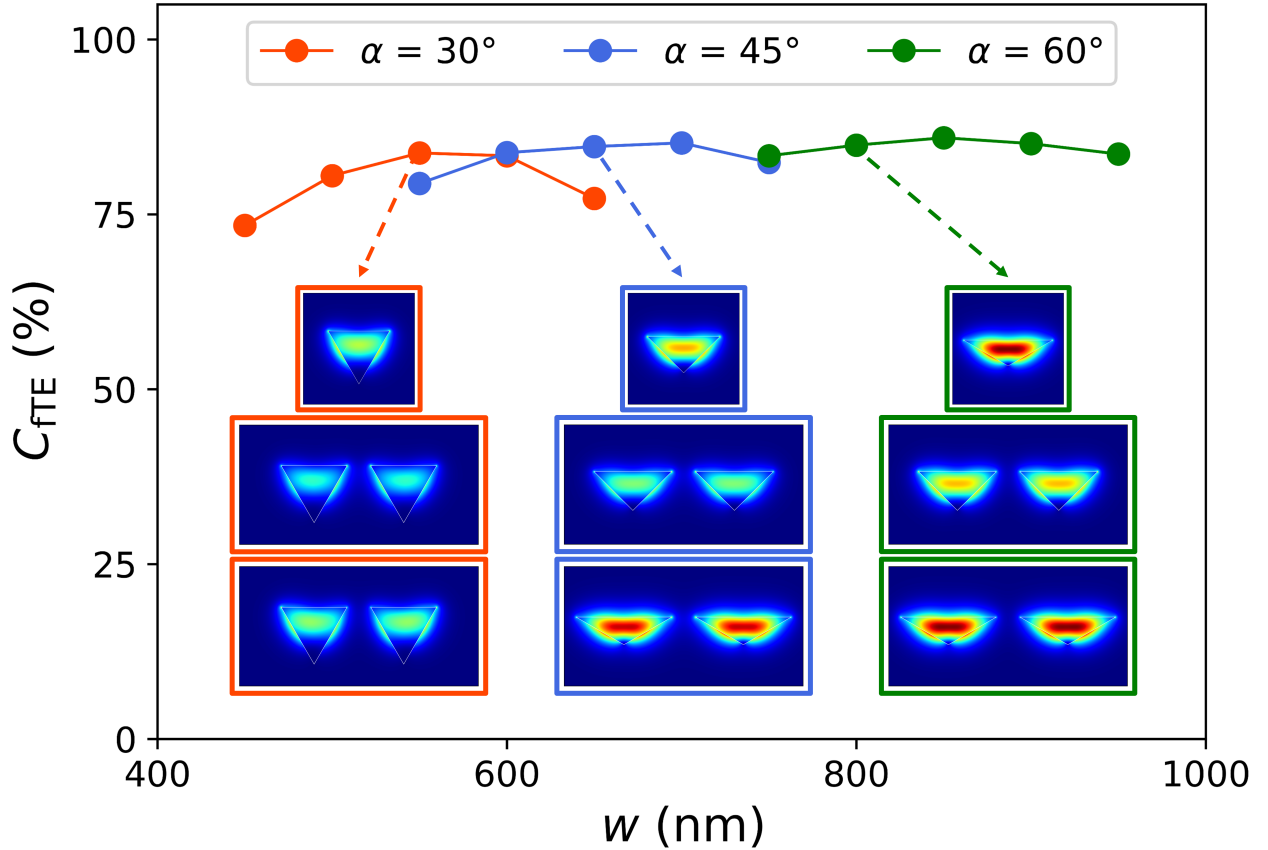


Figure 1: The coupling of a TE oriented dipole emission at the centroid of the triangular profile into the f-TE mode ( $C_{\text{fTE}}$ ) as a function of the waveguide width for three etch angles ( $\alpha$ ). Insets show electric field intensity profiles of the f-TE mode, TE supermode 1 and TE supermode 2 (top to bottom), at optimal waveguide widths supporting single mode propagation, for  $\alpha = 30^\circ, 45^\circ, 60^\circ$ . The electric field intensity of the TE supermodes were plotted for adjacent identical waveguides with 200 nm gap between them.

The mode profile of the waveguide f-TE (f-TM) mode has a E-field intensity maximum closer to the top surface (apex) [24]. As the waveguide width decreases, the E-field intensity maximum of the f-TM mode moves closer to the apex and becomes evanescent (not supported in the waveguide). Using MODE package in Lumerical software, we find that at these optimal widths for  $\alpha = 45^\circ$  and  $60^\circ$ , the waveguide supports only the f-TE mode. However, for  $\alpha = 30^\circ$ , both f-TE and f-TM modes are supported in the waveguide at the optimal and smaller widths. The height of the triangle varies inversely with  $\alpha$  and hence the widths needed for the f-TM to become evanescent are much smaller than the optimal width for  $\alpha = 30^\circ$ .

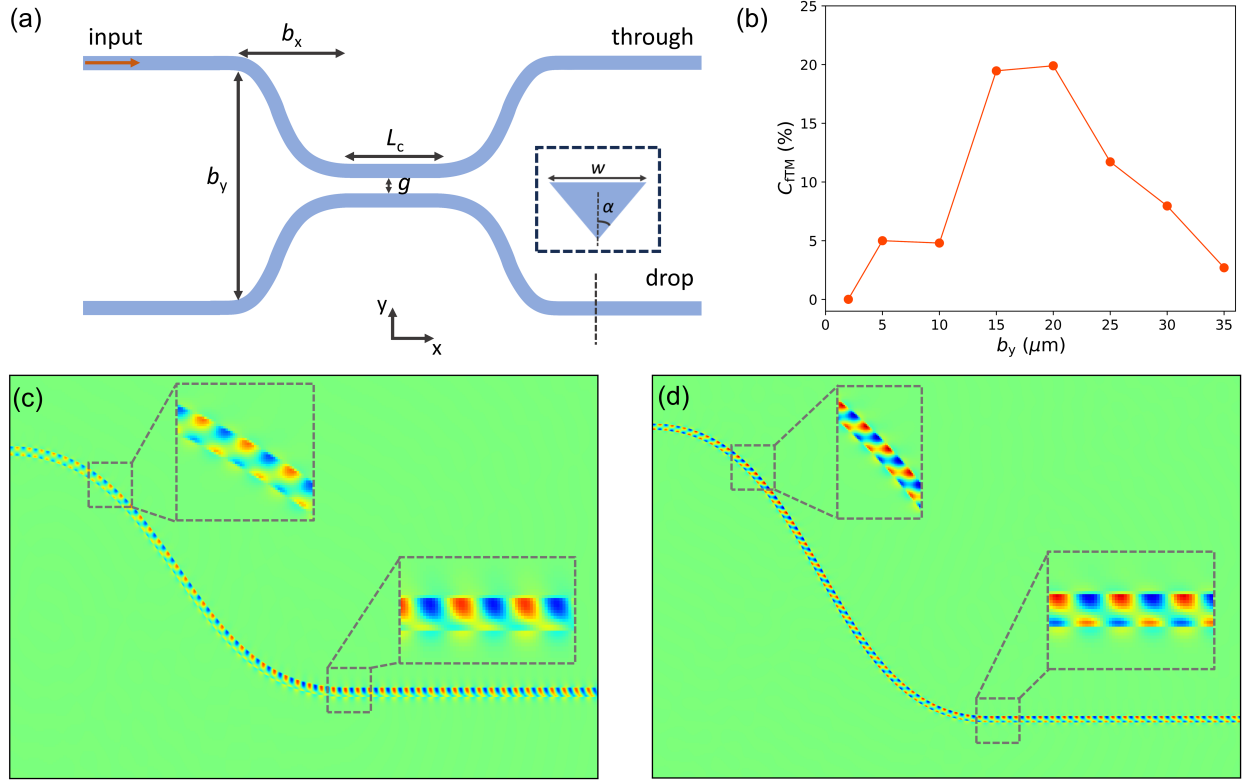


Figure 2: (a) Top view of the S-bend BS in 4H-SiC and the inset shows the triangular cross-section geometry. (b) The fraction of the f-TE input mode coupling to f-TM ( $C_{fTM}$ ) mode along the bend with variations in bend y-span ( $b_y$ ) for  $\alpha = 30^\circ$ ,  $w = 550 \text{ nm}$ , and  $L_C = 30 \mu\text{m}$ . (c)-(d) Propagation of  $E_z$  field in the  $xy$  plane of the structure described in (b) for  $b_y$  values of  $20 \mu\text{m}$  and  $35 \mu\text{m}$ , respectively.

In this paper, we design a 50:50 BS using two identical triangular cross-section waveguides

with three regions: 1) input and output - where the waveguides are far apart with zero electromagnetic interaction, on either ends of the BS, 2) bent waveguide region, and 3) coupling region - where the waveguides are close enough to electromagnetically interact, as shown in Figure 2a. When light is injected into the f-TE mode of one of the waveguides on the input side (top left), it propagates through the straight and bent regions of that waveguide. When it reaches the coupling region, some of the light in the top waveguide is coupled into the bottom waveguide as it propagates along. Then the light in both the waveguides pass through the bent and straight regions to reach the output ports (through and drop ports). The proportion of light coupled into the bottom waveguide is determined by the coupling strength between the individual waveguide modes and the length of the waveguides in the coupling region.

When two identical waveguides are close to each other, the individual modes (f-TE) in each of the waveguides superimpose to form a supermode. The coupling between the two waveguides can be analyzed in terms of a pair of TE supermodes, as shown in the inset of Figure 1. For a BS with power  $P_0$  in one of the waveguide at the beginning of the coupling region, the coupling length ( $L_C$ ) required for a power  $P_2$  to couple into the other waveguide is given by:

$$L_C = \frac{\lambda_0}{\pi \Delta n_{\text{eff}}} \sin^{-1} \sqrt{\frac{P_2}{P_0}} \quad (1)$$

where  $\lambda_0$  is the free space wavelength,  $\Delta n_{\text{eff}}$  is the difference in effective refractive indices of the two TE supermodes [29]. The coupling length is inversely proportional to the coupling strength between the waveguides given by  $\Delta n_{\text{eff}}$ , which in turn depends on the confinement of the individual waveguide modes and gap between the individual waveguides in the coupling region. For a 50:50 BS, where there is 50% light in both the waveguides after the coupling region, the ratio  $P_2/P_0$  equals 0.5. We use MODE package in Lumerical software to estimate the effective index of the two TE supermodes, for calculating the theoretical values of  $L_C$  for various BS geometries studied in the following section.

### 3 Integrated 4H-SiC beam splitter in triangular geometry

Recent advances in on-chip splitting mostly include rectangular or slab waveguides [15]. For performing QIP with integrated color centers in 4H-SiC, we construct the BS structure with symmetric triangular cross-section single mode S-bend waveguides with an overlap region to enable DC. Figure 2a shows the top view schematic of the BS with coupling length  $L_C$ , gap between the waveguides in the coupling region  $g$ , S-bend x-span  $b_x$ , S-bend y-span  $b_y$ , and the inset shows the triangular waveguide cross-section with  $w$  and  $\alpha$ . In this paper, we investigate 50:50 BS in triangular cross-section waveguides with  $\alpha = 30^\circ, 45^\circ, 60^\circ$ , can be fabricated with the state-of-the-art processes, by varying the gap  $g$  between waveguides and consequently  $L_C$ .

In Lumerical FDTD simulations (mesh size = 30 nm), we choose 20  $\mu\text{m}$  for  $b_x$  and 10  $\mu\text{m}$  for  $b_y$ , where  $b_x$  corresponds to the terminal points and  $b_y$  corresponds to the curvature control points of the S-bend (Bézier curve), for  $\alpha = 45^\circ, 60^\circ$ . For  $\alpha = 30^\circ$ , we need to account for potential higher-order mode conversion due to the bending curvature as the  $n_{\text{eff}}$ , one of the most important parameters for understanding mode propagation, of the f-TE and the f-TM modes are virtually the same in the waveguides with  $\alpha = 30^\circ$ . Hence, the f-TE mode can transform into the f-TM due to identical  $n_{\text{eff}}$  and inter-mode coupling via bends [30]. Keeping  $b_x = 20 \mu\text{m}$  constant, we vary  $b_y$  for modulating the bend curvature of the  $\{\alpha, w, L_C\} = \{30^\circ, 550 \text{ nm}, 30 \mu\text{m}\}$  BS structure.

To test the inter-mode coupling (cross-talk), we inject via the f-TE mode at the input port and collect via the f-TM mode at the through port of the BS. It is observed in Figure 2b that coupling to the f-TM mode ( $C_{\text{fTM}}$ ) initially increases with the increase in  $b_y$  and after reaching a maximum value of  $\sim 20\%$  for  $b_y = 20 \mu\text{m}$ ,  $C_{\text{fTM}}$  gradually decreases dropping down to 2.7% with  $b_y = 35 \mu\text{m}$ . This trend occurs due to the expansion of the curved path with increasing  $b_y$ , however, after the inversion point, the bending becomes so gradual that the S-bend mimics a straight path. For a better understanding of the f-TE and f-TM mode coupling, we also study the  $E_z$  fields of the minimum and maximum  $C_{\text{fTM}}$  as  $E_z$  field is a

good indicator of the existence of the TE and TM modes [25]. Figure 2c shows that at the starting point of the bending region with  $b_y = 20 \mu\text{m}$ ,  $E_z$  has a nodal plane in the triangular waveguide which corresponds to the f-TE mode and at the ending point,  $E_z$  field starts to develop in the waveguide, confirming the coupling to the f-TM mode. On the other hand, for  $b_y$  value of  $35 \mu\text{m}$ , there is a constant  $E_z$  nodal plane indicating the f-TE mode throughout the S-bend, depicted in Figure 2d, which makes this bend structure suitable for maintaining the single mode propagation in the BS.

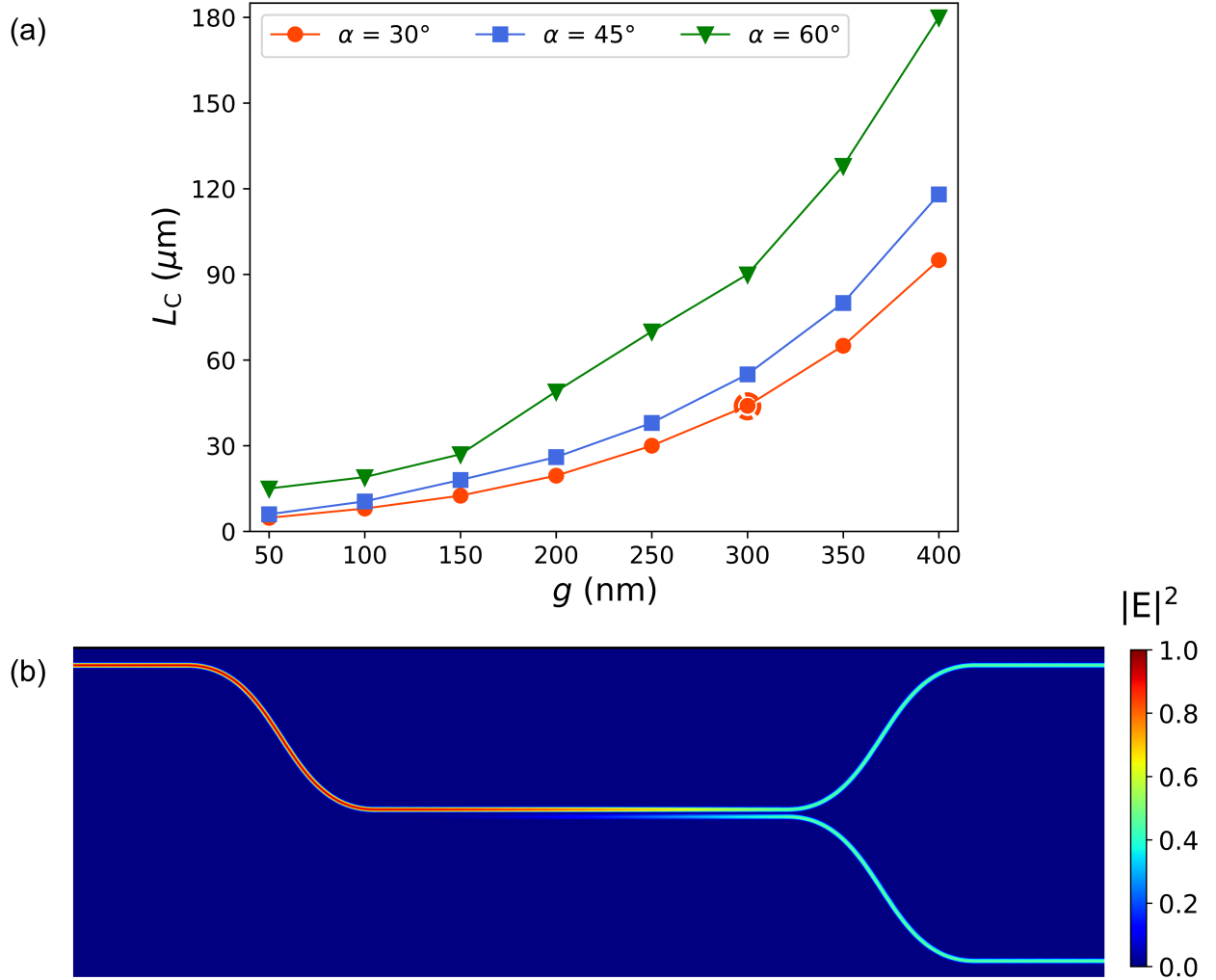


Figure 3: (a)  $L_C$  values for 50:50 splitting with an increasing gap  $g$  in  $\alpha = 30^\circ, 45^\circ, 60^\circ$  BS. (b) Top view of the  $E$ -field intensity profile for the integrated 50:50 BS SiC structure with  $\{\alpha, w, b_x, b_y, g, L_C\} = \{30^\circ, 550 \text{ nm}, 20 \mu\text{m}, 35 \mu\text{m}, 300 \text{ nm}, 44 \mu\text{m}\}$  indicated by dashed circle in Figure 3a.

The above discussions lead us to the optimal selection of  $w$  and  $b_y$  of the 50:50 BS for each  $\alpha$ . We choose 650 nm and 800 nm as  $w$  for  $\alpha = 45^\circ, 60^\circ$  respectively with  $b_y = 10 \mu\text{m}$  in order to maximize the coupling and maintain single mode propagation for establishing a suitable environment for QIP with the triangular cross-section BS. For  $\alpha = 30^\circ$  waveguides, we pick  $w = 550 \text{ nm}$  and  $b_y = 35 \mu\text{m}$  to achieve similar outcomes. We vary the gap  $g$  from 50 nm to 400 nm for exploring a range of designs. Figure 3a shows that with increasing  $g$ ,  $L_C$  shoots up rapidly for all three etch angles, experiencing minor losses ( $< 1.5\%$ ) upon propagation through the entire BS. We observe another interesting phenomenon that  $L_C$  for the 50:50 BS with  $\alpha = 60^\circ$  is dramatically longer than the  $\alpha = 30^\circ$  and  $\alpha = 45^\circ$  BS for a particular  $g$  when  $g \geq 200 \text{ nm}$ . As a result, owing to smaller footprints,  $\alpha = 30^\circ$  and  $\alpha = 45^\circ$  BS appear as better candidates than the  $\alpha = 60^\circ$  BS for integrated quantum mesh photonic circuitry.

## 4 Fabrication of closely spaced triangular waveguides in 4H-SiC

Triangular cross-section photonics has previously been fabricated in SiC through Faraday cage assisted etching method [16, 18, 22] suitable for chip-scale integration of color centers with no degradation in color-center properties compared to bulk substrate [18]. This approach could be brought to wafer-scale using the ion beam etching [23]. Therefore, we test a new ion beam etching process to fabricate triangular cross-section waveguides in 4H-SiC [31], with varying gaps between waveguides (100 nm, 200 nm, 300 nm, 500 nm). This provides an insight into what spacing between the waveguides in the coupling region of the simulated 50:50 BS are fabrication friendly, using the ion beam etch process.

We use electron beam lithography to define the patterns on 4H-SiC substrates and then the pattern is transferred to a 120 nm thick nickel hard mask deposited using an electron beam evaporation, through a lift-off process. Triangular cross-section waveguides are then fabricated by ion beam etch using  $\text{SF}_6$  and  $\text{O}_2$  chemistry. We use focused ion beam (FIB) - scanning electron microscope (SEM) to confirm the triangular cross-section of the fabricated

waveguides, as shown in the inset of Figure 4d. We measure the etch angle ( $\alpha$ ) of these waveguides to be  $30^\circ$ . For adjacent waveguides with gaps of 100 nm and 200 nm, we observe no substantial etch in the region between the waveguides, as shown in Figure 4a-b. For waveguide gaps  $\geq 300$  nm (300 nm, 500 nm), the fabricated waveguides have triangular cross-sections, as shown in Figure 4c-d. The lack of etching in the region between the waveguides for smaller waveguide gaps may be due to the inability of the ions which are incident at an angle on the substrate, to reach well below the surface level of the substrate, and also reduced etching caused by mass-transport issues in those closely spaced regions.

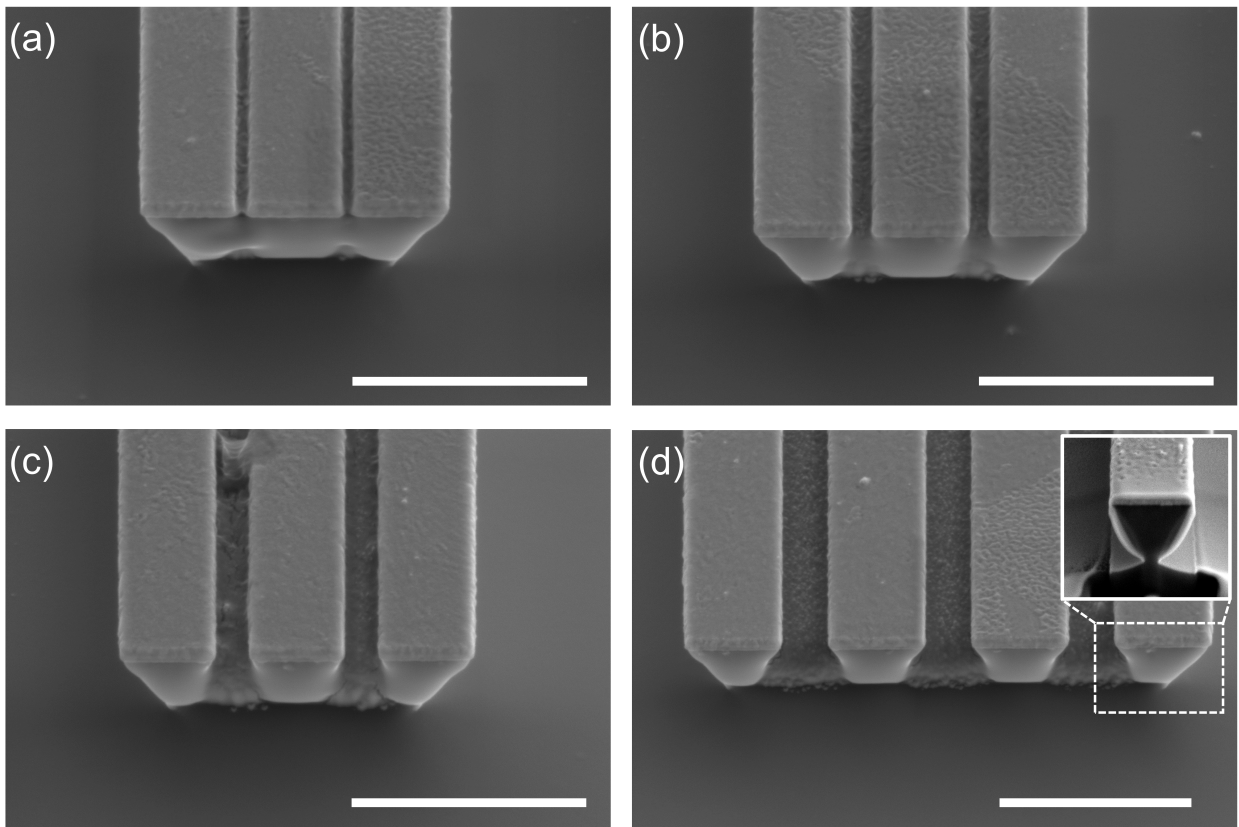


Figure 4: The SEM images of ion beam etched waveguides in 4H-SiC. (a)-(c) 800 nm wide waveguides with gaps of 100 nm, 200 nm and 300 nm respectively. (d) 1000 nm wide waveguides with a gap of 500 nm. Inset shows a FIB-SEM of the fabricated 1000 nm waveguide with a triangular cross-section. The scale bar is  $2 \mu\text{m}$ .

## 5 Discussion

The modeling results presented in this paper offer an approach to build low-loss triangular cross-section 50:50 BS in 4H-SiC necessary to perform key quantum interferometry operations for QIP applications. Here, triangular cross-section photonics provide a scalable route to integrate color centers into quantum photonic devices and circuits. Moreover, high-performance triangular cross-section photonic structures in 4H-SiC like waveguides, waveguides with integrated SNSPDs, photonic crystal mirrors, and photonic crystal cavities that facilitate efficient generation, collection and detection of single photon emission from color centers, necessary for applications in QIP have been demonstrated [12, 18, 24, 25]. Thereby, NV center in 4H-SiC with emission wavelengths near the telecommunications range is most suited for building large-scale quantum communication networks.

Our initial fabrication tests show that triangular cross-section waveguides with gaps greater than 300 nm can be fabricated using the wafer-scale ion beam etch process. From the simulations, we note that for a waveguide gap  $g \geq 300$  nm in the coupling region,  $\alpha = 30^\circ$  and  $45^\circ$ , offer 50:50 BS with fabricatable footprints (e.g. coupling region  $L_C \leq 50$   $\mu\text{m}$ ), for applications in QIP. Here, supporting structures for waveguide suspension would need to be designed. The ion beam etch process conditions could be further optimized to achieve triangular cross-section waveguides with waveguide gap  $\leq 300$  nm, by choosing process conditions that result in a predominantly chemical etch. Under such etch conditions, the byproducts of the etch are volatile gases ( $\text{SiF}_4$ ,  $\text{CO}$ ,  $\text{CO}_2$ ), preventing re-deposition, allowing the etch to continue. When there is a reasonable physical etch component, the sputtered material has a higher chance of re-deposition, especially when the gap between the waveguides is small, resulting in a slower etch or sometimes no etch. Another alternative could be choosing a steeper etch angle, because such waveguides would not require a deep etch to release the structure.

Triangular cross-section photonics in 4H-SiC provides an avenue to achieve efficient chip- and wafer-scale integration of color centers, with very little degradation of color center properties compared to bulk, essential for applications in QIP. Our simulation results demonstrate that 50:50 BS necessary for applications in QIP can be implemented using



triangular geometry and our initial etch tests show that ion beam etching is suitable for achieving this.

## 6 Acknowledgments

M.R., S.M. and P.S. acknowledge support from NSF CAREER (Award 2047564) and AFOSR Young Investigator Program (Award FA9550-23-1-0266). Z.K. acknowledges support by CITRIS Workforce Innovation Program. Work at the Molecular Foundry was supported by the Office of Science, Office of Basic Energy Sciences, of the U.S. Department of Energy under Contract No. DE-AC02-05CH11231. Part of this study was carried out at the UC Davis Center for Nano and Micro Manufacturing (CNM2).

## References

- [1] Victoria A Norman, Sridhar Majety, Zhipan Wang, William H Casey, Nicholas Curro, and Marina Radulaski. Novel color center platforms enabling fundamental scientific discovery. *InfoMat*, 3(8):869–890, 2021.
- [2] Marianne Etzelmüller Bathen and Lasse Vines. Manipulating single-photon emission from point defects in diamond and silicon carbide. *Advanced Quantum Technologies*, 4(7):2100003, 2021.
- [3] Nguyen T Son, Christopher P Anderson, Alexandre Bourassa, Kevin C Miao, Charles Babin, Matthias Widmann, Matthias Niethammer, Jawad Ul Hassan, Naoya Morioka, Ivan G Ivanov, et al. Developing silicon carbide for quantum spintronics. *Applied Physics Letters*, 116(19), 2020.
- [4] Stefania Castelletto and Alberto Boretti. Silicon carbide color centers for quantum applications. *Journal of Physics: Photonics*, 2(2):022001, 2020.
- [5] Daniil M Lukin, Melissa A Guidry, and Jelena Vučković. Integrated quantum photonics with silicon carbide: challenges and prospects. *PRX Quantum*, 1(2):020102, 2020.

- [6] Sridhar Majety, Pranta Saha, Victoria A Norman, and Marina Radulaski. Quantum information processing with integrated silicon carbide photonics. *Journal of Applied Physics*, 131(13), 2022.
- [7] Ryan Hamerly, Saumil Bandyopadhyay, and Dirk Englund. Asymptotically fault-tolerant programmable photonics. *Nature Communications*, 13(1):6831, 2022.
- [8] Mark Dong, Matthew Zimmermann, David Heim, Hyeonrak Choi, Genevieve Clark, Andrew J Leenheer, Kevin J Palm, Alex Witte, Daniel Dominguez, Gerald Gilbert, et al. Programmable photonic integrated meshes for modular generation of optical entanglement links. *npj Quantum Information*, 9(1):42, 2023.
- [9] Wim Bogaerts, Daniel Pérez, José Capmany, David AB Miller, Joyce Poon, Dirk Englund, Francesco Morichetti, and Andrea Melloni. Programmable photonic circuits. *Nature*, 586(7828):207–216, 2020.
- [10] Samuel Gyger, Julien Zichi, Lucas Schweickert, Ali W Elshaari, Stephan Steinhauer, Saimon F Covre da Silva, Armando Rastelli, Val Zwiller, Klaus D Jöns, and Carlos Errando-Herranz. Reconfigurable photonics with on-chip single-photon detectors. *Nature Communications*, 12(1):1408, 2021.
- [11] F Martini, A Gaggero, F Mattioli, and R Leoni. Single photon detection with superconducting nanowires on crystalline silicon carbide. *Optics Express*, 27(21):29669–29675, 2019.
- [12] Sridhar Majety, Stefan Strohauer, Pranta Saha, Fabian Wietschorke, Jonathan J Finley, Kai Müller, and Marina Radulaski. Triangular quantum photonic devices with integrated detectors in silicon carbide. *Materials for Quantum Technology*, 3(1):015004, 2023.
- [13] Michael Reck, Anton Zeilinger, Herbert J Bernstein, and Philip Bertani. Experimental realization of any discrete unitary operator. *Physical Review Letters*, 73(1):58, 1994.
- [14] Emanuel Knill, Raymond Laflamme, and Gerald J Milburn. A scheme for efficient quantum computation with linear optics. *Nature*, 409(6816):46–52, 2001.

- [15] Yuting Xu, Zhongxing Tian, Xiaoqin Meng, and Zhen Chai. Methods and applications of on-chip beam splitting: A review. *Frontiers in Physics*, 10:985208, 2022.
- [16] Michael J Burek, Nathalie P De Leon, Brendan J Shields, Birgit JM Hausmann, Yiwen Chu, Qimin Quan, Alexander S Zibrov, Hongkun Park, Mikhail D Lukin, and Marko Lončar. Free-standing mechanical and photonic nanostructures in single-crystal diamond. *Nano Letters*, 12(12):6084–6089, 2012.
- [17] Jonathan M Kindem, Andrei Ruskuc, John G Bartholomew, Jake Rochman, Yan Qi Huan, and Andrei Faraon. Control and single-shot readout of an ion embedded in a nanophotonic cavity. *Nature*, 580(7802):201–204, 2020.
- [18] Charles Babin, Rainer Stöhr, Naoya Morioka, Tobias Linkewitz, Timo Steidl, Raphael Wörnle, Di Liu, Erik Hesselmeier, Vadim Vorobyov, Andrej Denisenko, et al. Fabrication and nanophotonic waveguide integration of silicon carbide colour centres with preserved spin-optical coherence. *Nature Materials*, 21(1):67–73, 2022.
- [19] Gabriel Ferro. 3C-SiC heteroepitaxial growth on silicon: the quest for holy grail. *Critical Reviews in Solid State and Materials Sciences*, 40(1):56–76, 2015.
- [20] David O Bracher, Xingyu Zhang, and Evelyn L Hu. Selective purcell enhancement of two closely linked zero-phonon transitions of a silicon carbide color center. *Proceedings of the National Academy of Sciences*, 114(16):4060–4065, 2017.
- [21] Daniil M Lukin, Constantin Dory, Melissa A Guidry, Ki Youl Yang, Sattwik Deb Mishra, Rahul Trivedi, Marina Radulaski, Shuo Sun, Dries Vercruyssen, Geun Ho Ahn, et al. 4H-silicon-carbide-on-insulator for integrated quantum and nonlinear photonics. *Nature Photonics*, 14(5):330–334, 2020.
- [22] Bong-Shik Song, Seungwoo Jeon, Heungjoon Kim, Dongyeon Daniel Kang, Takashi Asano, and Susumu Noda. High-Q-factor nanobeam photonic crystal cavities in bulk silicon carbide. *Applied Physics Letters*, 113(23), 2018.

- [23] Haig A Atikian, Pawel Latawiec, Michael J Burek, Young-Ik Sohn, Srujan Meesala, Normand Gravel, Ammar B Kouki, and Marko Lončar. Freestanding nanostructures via reactive ion beam angled etching. *APL Photonics*, 2(5), 2017.
- [24] Sridhar Majety, Victoria A Norman, Liang Li, Miranda Bell, Pranta Saha, and Marina Radulaski. Quantum photonics in triangular-cross-section nanodevices in silicon carbide. *Journal of Physics: Photonics*, 3(3):034008, 2021.
- [25] Pranta Saha, Sridhar Majety, and Marina Radulaski. Utilizing photonic band gap in triangular silicon carbide structures for efficient quantum nanophotonic hardware. *Scientific Reports*, 13(1):4112, 2023.
- [26] Zhao Mu, Soroush Abbasi Zargaleh, Hans Jurgen von Bardeleben, Johannes E Fröch, Milad Nonahal, Hongbing Cai, Xinge Yang, Jianqun Yang, Xingji Li, Igor Aharonovich, et al. Coherent manipulation with resonant excitation and single emitter creation of nitrogen vacancy centers in 4H silicon carbide. *Nano Letters*, 20(8):6142–6147, 2020.
- [27] Shin-ichiro Sato, Takuma Narahara, Yuta Abe, Yasuto Hijikata, Takahide Umeda, and Takeshi Ohshima. Formation of nitrogen-vacancy centers in 4H-SiC and their near infrared photoluminescence properties. *Journal of Applied Physics*, 126(8), 2019.
- [28] Carlton M Caves and Peter D Drummond. Quantum limits on bosonic communication rates. *Reviews of Modern Physics*, 66(2):481, 1994.
- [29] Wu Yuan, Graham E Town, and Ole Bang. Refractive index sensing in an all-solid twin-core photonic bandgap fiber. *IEEE Sensors Journal*, 10(7):1192–1199, 2010.
- [30] Long Zhang, Lanlan Jie, Ming Zhang, Yi Wang, Yiwei Xie, Yaocheng Shi, and Daoxin Dai. Ultrahigh-Q silicon racetrack resonators. *Photonics Research*, 8(5):684–689, 2020.
- [31] Sridhar Majety, Pranta Saha, and Marina Radulaski. Wafer-scale fabrication of quantum photonic devices in silicon carbide. In *Laser Science*, pages JTU5A–40. Optica Publishing Group, 2023.